Small-Angle X-ray Scattering and Light Scattering on Lysozyme and Sodium Glycocholate Micelles

Claudia Leggio,[†,‡] Luciano Galantini,*[,†,‡] Emanuela Zaccarelli,[‡,§] and Nicolae Viorel Pavel[†,‡]

Dipartimento di Chimica, Research Center SOFT-INFM-CNR, and Dipartimento di Fisica, Università di Roma "La Sapienza", P.le A. Moro 5, 00185 Roma, Italy

Received: July 1, 2005; In Final Form: October 19, 2005

Small-angle X-ray scattering (SAXS) together with static (SLS) and dynamic light scattering (DLS) measurements were carried out on aqueous solutions of lysozyme (LY) and of the ionic biological detergent sodium glycocholate (NaGC). Apparent diffusion coefficients (D_{app}), excess Rayleigh ratio, and SAXS spectra were measured for 0.1 M NaGC solutions at different ionic strengths (0.05−0.30 M NaCl). The same data were collected for LY in sodium acetate buffer 50 mM without and with 92 mM NaCl as a function of protein concentration (10−80 g L^{-1}). A correlated analysis of SLS data and SAXS spectra was first tested on the LY samples and then extended to the interpretation of the NaGC data to infer information on particle structure and interaction potential. A hard-core (HC) interaction shell of uniform thickness, a screened Coulomb potential of the electric double layer (EDL) or the complete DLVO potential were alternatively used to represent the long-range tail of the interaction potential. Whenever an essentially repulsive tail is expected, all the representations give reasonable results, but the data analysis does not allow the discrimination between the oblate and the prolate symmetries of the NaGC aggregates. The DLVO model allows the interpretation of the data even when the attractive component determines the tail character. With this model an overall fit of the micelle data at all the NaCl concentrations was successfully performed by assuming a simple spherical symmetry of the micelles and invariant values of their ionization degree and Hamaker constant, thus considering just the screening effect of the added electrolyte. Whatever model is used, the results point out that the aggregates are quite hydrated (26−38 water molecules per monomer) and very slightly grow by increasing the NaCl concentration. When spherical symmetry is assumed the aggregate radii for all the samples fall in the range 15−16 Å. From the SAXS and SLS, best fitting geometrical parameters, and interparticle structure factor, a D_{app} value was calculated for each sample. An excellent consistence is achieved for LY results. On the contrary, calculated D_{app} values systematically lower than the experimental values are always obtained for the NaGC micelles. Micelle polydispersity and internal dynamics seem to be the most probable reasons of the bad agreement.

Introduction

Particle structure and particle interaction potential are fundamental properties to rationalize the physical chemistry of colloids. For this purpose, transport property measurements, such as those performed by dynamic light scattering (DLS) as well as static scattering data, such as those provided by static light scattering (SLS) and small-angle X-ray scattering (SAXS), are often used. Obviously the particle interaction effect on the experimental data is detectable and can be reliably analyzed when concentrated systems are studied. However, this effect is regarded as a nuisance when the investigation interest is essentially focused on the particle structure and is generally removed by extrapolating the data at infinite dilution.

When the wavelength and the particle size are comparable, the static scattering pattern is a function of the distribution of the scattering centers within the particle and of the particle distribution within the solution. In this case, a rough description of the particle structure and interaction potential can be inferred by analyzing the angular dependence of the scattered intensity for concentrated samples, thus avoiding the extrapolation at infinite dilution.[1−4] For micellar systems at the most commonly studied concentrations this condition is generally realized when X-ray or neutron scattering measurements are performed. On the contrary, when the visible light is used as in SLS and DLS experiments, no angular dependence of the scattering data is observed since the wavelength is generally much greater than both the particle size and the mean interparticle distances.

In this case SLS and DLS studies are performed by analyzing only the concentration dependence of the experimental data. Therefore, the information on particle structure and particle interactions is inferred from the intercept and the slope of the experimental trend in the dilute region.[5−11]

Actually, the extrapolation procedure can be unreliable when micellar solutions are studied since very often the micelles change their size and shape by changing the surfactant concentration. The problem is more complicated in the case of ionic micelle solutions, where both the micellar structure and the particle interaction potential depend on the ionic strength since this parameter varies with the surfactant concentration and, also, can be changed by the addition of a different electrolyte.[1−3,12,13]

* Author to whom correspondence should be addressed. Phone: (+39)-06-49913687. Fax: (+39)-06-490631. E-mail: l.galantini@caspur.it.
[†] Dipartimento di Chimica.
[‡] Research Center SOFT-INFM-CNR.
[§] Dipartimento di Fisica.

10.1021/jp053603b CCC: $30.25
Published on Web 11/22/2005

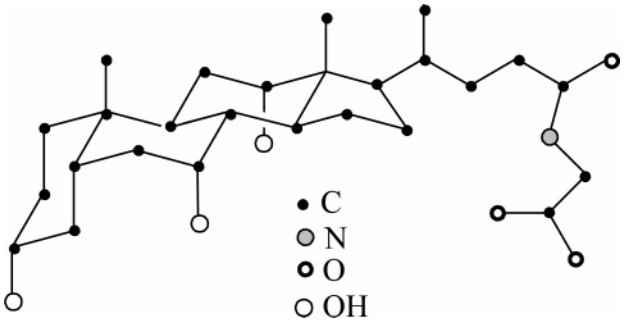

Figure 1. Molecular formula of the glycochotate anion (hydrogen atoms are omitted).

However, a correlated analysis of SAXS, SLS, and DLS data can be performed in which the information on particle distribution, obtained from the SAXS data, is used to interpret SLS and DLS results, thus avoiding the extrapolation method. The main results of this kind of analysis can be summarized in two major points. The first is that in this way more realistic descriptions of structure and interactions of unknown particles can be provided by interpreting the data obtained from the different techniques. Moreover, when applied to particles of known structure, the consistency of the data analysis given by different techniques can be used to test the models and the approximations that are normally involved in the interpretation of the experimental data.

Recently this kind of approach was used in the interpretation of SAXS and DLS data of some bile acid salts, sodium glycodeoxycholate (NaGDC)[14] and taurodeoxycholate (NaTDC).[15] The bile salts are extremely important biological surfactants, which guarantee the solubilization of a wide variety of molecules in aqueous physiological solutions. Because of their biological importance the physicochemical characterization of bile salt micelles represents a quite interesting topic. In particular, significant work has been dedicated to the determination of the micellar aggregate structure.[11,14−28] The reason is that the amphiphilic nature of bile salts depends on a peculiar disposition of polar and apolar groups in their molecules (Figure 1), and then the structures of their aggregates are quite different from those of classical detergents.

In this paper, the complete correlation of SAXS, SLS, and DLS data is reported. This integrated analysis is first tested on the lysozyme (LY) solutions that we chose as model systems. Hence, it is extended to the study of bile salt (sodium glycocholate, NaGC, Figure 1) micellar solutions over a NaCl concentration range of 0.05−0.30 M.

Experimental Section

Materials. NaGC (Sigma), LY from chicken egg white crystallized 3 times, dialized, and lyophilized (Sigma), and NaCl (Merck, suprapur) were used. NaGC was crystallized from a mixture of water and acetone and dried under vacuum. The pH 4.75 acetate buffer (NaAc buffer) was prepared by mixing equal amounts of sodium acetate and acetic acid. The final concentrations of the two species in the buffer solution were 50 mM. After the protein addition the pH of each sample was corrected by adding very small amounts of concentrated acetic acid. The total volume variation, which is given by this correction, was neglected in the calculation of the final concentration of the ionic species in the medium. The actual LY concentrations in the samples were determined by UV absorption measurements using $\epsilon_{280} = 2.64$ mL mg^{-1} cm^{-1}.

SAXS Measurements. The SAXS measurements were carried out in a 1-mm quartz capillary by using a Kratky compact camera, containing a slit collimation system, equipped with a NaI scintillation counter, in a temperature-controlled room at 25 ± 1 °C. Ni-filtered Cu Kα radiation ($\lambda = 1.5418$ Å) was used. Scattering curves were recorded within the range $0.012 \le q \le 0.5$ Å^{-1} ($q = 4\pi \sin(\theta/\lambda)$). The moving slit method was employed to measure the intensity of the primary beam. The collimated scattering intensities were put on an absolute scale and thus expressed in electron units, e.u. (electrons^2 Å^{-3}) per centimeter of primary beam length.[29,30] In terms of total scattering cross section of an ensemble of particles, 1 e.u. corresponds to 7.94056×10^{-2} cm^{-1}.[31] In the minimization procedures, the calculated intensities have been smeared by the normalized weighting functions for slit length and slit width effects,[32] and the best agreement with the experimental data was obtained by minimizing the function

$$R = \frac{1}{N}\sum_{i=1}^{N}\frac{(Io_i(q) - Ic_i(q))^2}{\sigma_i^2}$$

where $Io_i(q)$ and $Ic_i(q)$ are the smeared observed and calculated intensities, σ_i^2 is the $Io_i(q)$ variance, and N is the number of experimental points.

SLS and DLS Measurements. In the SLS experiments the excess Rayleigh ratio of the sample, at the scattering vector q, was determined as $\Delta R(q) = R_{tol}[\langle I(q)\rangle - \langle I_s(q)\rangle]/\langle I_{tol}(q)\rangle$ where R_{tol} is the known toluene Rayleigh ratio and $\langle I(q)\rangle$, $\langle I_s(q)\rangle$, and $\langle I_{tol}(q)\rangle$ are the average intensities of sample, solvent, and toluene, respectively.

In the DLS measurements, the temporal fluctuations of the scattered intensity by a micellar solution were analyzed by estimating the normalized temporal autocorrelation function of the scattered intensity

$$g_2(q,\tau) = \frac{\langle I(q,0)I(q,\tau)\rangle}{\langle I(q)\rangle^2}$$

where $I(q,\tau)$ is the scattered intensity at the scattering vector q and at the time τ. By assuming a Gaussian distribution of the intensity profile, the normalized field autocorrelation function $g_1(q,\tau)$ was derived from $g_2(q,\tau)$ through the Siegert relation.[33,34] Therefore $g_1(q,\tau)$ was analyzed through the cumulant expansion, and the so-called apparent diffusion coefficient D_{app} was obtained from the first cumulant by the relation

$$D_{app} = -\frac{1}{q^2}\frac{\mathrm{d}\ln g_1(q,\tau)}{\mathrm{d}\tau}\Big|_{\tau=0}$$

A Brookhaven instrument constituted by a BI-2030AT digital correlator with 136 channels and a BI-200SM goniometer was used. The light source was a Uniphase solid-state laser system model 4601 operating at 532 nm. Dust was eliminated by means of a Brookhaven ultrafiltration unit (BIUU1) for flow-through cells, the volume of the flow cell being about 1.0 cm^3. Nuclepore filters with a pore size of 0.1 μm were used. The samples were placed in the cell for at least 30 min prior the measurement to allow for thermal equilibration. Their temperature was kept constant within 0.5 °C by a circulating water bath. The time-dependent light scattering correlation function was analyzed only at the 90° scattering angle. Apparent diffusion coefficients did not show any relevant dependence on the exchanged wave vector in the range 30−150° in our experimental conditions. Refractive index measurements for the NaGC SLS data inter-

pretation were performed by means of an Index Instruments refractometer GPR 11-37.

Theoretical Background

Interaction Potential Models. Several published results indicate that the particle direct interaction can be well approximated as a sum of a hard body repulsion or excluded volume component plus a long-range interaction tail. For spherical particles of radius a the hard body repulsion is defined as

$$V_{HS} = \infty \quad \text{for} \quad x < 1$$
$$= 0 \quad \text{for} \quad x > 1$$

where as a function of the interparticle absolute distance r we have $x = r/2a$. The DLVO theory of colloid stability[35] indicates that, for charged colloids, a suitable representation of the interaction tail is given by the superposition of an electric double layer repulsion (V_{EDL}) and a van der Waals attraction (V_a). In particular, from the solution of the Poisson−Boltzmann equation for the charged double layer, it suggests that the electrostatic repulsive component can be represented by a screened Coulomb potential. The analytical form of this potential depends on the value of the Debye−Hückel reciprocal screening length κ, which is defined as

$$\kappa = \left(\frac{2N_A e^2 I 10^3}{kT\epsilon\epsilon_0}\right)^{1/2} \tag{1}$$

where ϵ is the dielectric constant of the medium, ϵ_0 is the permittivity of the free space, e is the electronic charge, k is the Boltzmann constant, T is the absolute temperature, N_A is Avogadro's number, and I is the ionic strength defined as $I = {}^1/_2\sum_i c_i z_i^2$, with c_i and z_i representing the molarity and the charge number of each ion in the medium. When κ is sufficiently small or more quantitatively when $\kappa a \leq 3$, the electrostatic repulsion can be well approximated by a Yukawa potential. A potential tail in the general Yukawa form is given by

$$V(x) = \frac{J}{x}\exp\left[-2a\frac{(x-1)}{d}\right] \tag{2}$$

where d and J are the characteristic range and depth, respectively. For the DLVO Coulombic repulsion, V_{EDL}, we have $d = 1/\kappa$ and

$$J = \frac{Z^2 e^2}{8\pi\epsilon_o\epsilon a(1+\kappa a)^2} \tag{3}$$

where Ze is the particle charge.

A complete definition of the particle interaction potential tail needs the attractive van der Waals contribution to be added to the electrostatic repulsive one. For this component the following expression derived by Hamaker[36] is available

$$V_a = -\frac{A}{12}\left[\frac{1}{x^2-1} + \frac{1}{x^2} + 2\ln\left(\frac{x^2-1}{x^2}\right)\right] \tag{4}$$

where A is the Hamaker constant. The potential diverges when $x = 1$, so a lower cutoff representing a steric protection thickness must be assumed to suppress the divergence.

To overcome problems in calculations, sometimes a Yukawa form is also used to represent the particle attractive component.[37,38] The choice of J (J_{att}) and d (d_{att}) in this potential is strictly related to the particle A value and to the steric protection thickness that would be assumed for the Hamaker equation. When protein solutions are treated, a potential of mean force constituted by the DLVO expression plus two further contributions is employed to describe the particle interactions. These contributions are expressed by a component accounting for self-association of proteins and an osmotic attractive potential due to the excluded volume effect of the salt ions, which is extremely important when solutions with high concentrations of added electrolyte are considered.[37,39] In the latter condition satisfactory fits of SAXS, SLS, and DLS data can be achieved if the Yukawa form of the attractive component is supposed to account for both the van der Waals and the osmotic attractive contributions.[37]

However, at low added electrolyte concentration, as in our case, the osmotic contribution in LY solutions can be neglected, and the complete DLVO potential ($V = V_{HS} + V_{EDL} + V_a$) is exhaustive to model the interaction between colloidal charged particles (DLVO interaction model).[37,38] Therefore we used this potential as the most reliable to discuss our results.

In any case, depending on the experimental conditions, much simpler forms for the interaction potential can be employed. In particular, whenever the electrostatic repulsion effect prevails over the attractive one, the whole interaction potential can be considered as a sum of the hard body component plus a long-range tail with an effective repulsive character. Very often in this case the attractive component of the DLVO model is neglected, and the hard body component with an electric double layer potential tail, expressed as in eqs 1−3, is used to describe the micelle−micelle interaction potential ($V = V_{HS} + V_{EDL}$) (EDL interaction model).[1−4,40−46]

Alternatively, a very simple hard-core (HC) interaction model can be applied where the effect of particle interactions is mimicked by representing the potential tail as a rigid interaction shell of suitable thickness t.[14−18,47,48] In this way, spherical particles are supposed to give a hard-core interaction at a radius $a + t$, where a is the particle radius. For ellipsoidal particles, a homogeneous thickness of the interaction shell can be considered. This means that for particles with semiaxes a_e and b_e an interaction ellipsoid of semiaxes $a_e + t$ and $b_e + t$, t being the interaction shell thickness, is assumed.

The EDL and the HC models have been already used in the correlation of SAXS and DLS data on NaGDC[14] and NaTDC[15] micellar solutions. However, some inconsistencies have been observed in the data interpretation that throw some doubt on the validity of these models. Actually, a definitive conclusion on the reasons of this interpretation failure has not been reached. The problem is that when self-assembling systems are studied some aspects such as polydispersity and aggregate internal dynamics, which are usually present in these systems, affect the data analysis. Hence, the interpretation model influence on the results cannot be rationalized. Protein solutions do not present these problems and can be reliably used to test these models. For these reasons an analysis of well characterized LY solutions was performed in this work under the assumption of HC and EDL interaction potential. Moreover the more realistic DLVO model was applied, and finally, all three representations were employed to analyze NaGC solutions.

SAXS Data Treatment. The contribution of a single particle to the total scattered intensity $I(q)$ is generally expressed in terms of scattering form factor $F(q)$ defined as

$$F(q) = \int \Delta\rho \exp(iqr)\, dV$$

where $\Delta\rho$ is the difference between the particle and the solvent

electron density. The integral is over the volume V of the particle. For a monodisperse system of homogeneous and spherically symmetric particles, the intensity can be factored into separate intra- and interparticle functions as

$$I(q) = N_p P(q) S(q) \tag{5}$$

where N_p is the particle number density, $P(q)$ is the intraparticle structure factor that, for a homogeneous sphere with radius a, is given by

$$P(q) = |F(q)|^2 = \left[4\pi\Delta\rho \frac{\sin(qa) - qa\cos(qa)}{q^3}\right]^2 \tag{6}$$

and $S(q)$ is the interparticle structure factor that is related to the particle distribution within the solution and that, as a function of the particle volume fraction ϕ, can be expressed as

$$S(q) = 1 + 24\phi \int_0^\infty x^2[g(x) - 1]\frac{\sin 2aqx}{2aqx}\,dx \tag{7}$$

with $g(x)$ representing the radial distribution function. It is important to note that both N_p and ϕ can be expressed as a function of the particle molecular weight M as $N_p = cN_A/M$ and $\phi = 4\pi ca^3N_A/3M$, where c and N_A are the particle mass density and Avogadro's number, respectively. For nonspherically symmetric but monodispersed particles, the decoupling approximation can be assumed, and the scattered intensity expression can be generalized to[1-4]

$$I(q) = N_p\langle|F(q)|^2\rangle\left[1 + \frac{|\langle F(q)\rangle|^2}{\langle|F(q)|^2\rangle}(S(q) - 1)\right] \tag{8}$$

with the angular brackets representing the average over all the particle orientations. Generally oblate or prolate ellipsoids of revolution are used to describe the shape of micelles or globular macromolecules. The $F(q)$ average expressions for these geometries are widely reported in the literature.[4]

A detailed description of colloidal particle structure needs SAXS spectra to be collected for very dilute samples where particle interactions are negligible. In such a way, $S(q) = 1$ can be assumed, and the SAXS pattern can be interpreted as a function of particle structure alone. The indirect Fourier transform, as developed, for example, in the ITP program,[49] constitutes a very powerful method for analyzing the spectra in these conditions. Moreover, it is well established that the experimental SAXS patterns of native protein solutions can be adequately described by scattering curves calculated from crystallographic structures and accounting for hydration effects. A program (CRYSOL) able to evaluate SAXS profiles from crystallographic structures, taking into account a hydration shell contribution described by a border layer of variable scattering density, has been developed by Svergun et al.[50]

SLS and DLS Data Treatment. It is known that for a solution of small, interacting particles the excess Rayleigh ratio can be expressed as

$$\Delta R = cKMS(q) \tag{9}$$

with

$$K = \frac{4\pi^2 n_o^{\,2}}{N_A\lambda^4}\left(\frac{dn}{dc}\right)^2 \tag{10}$$

where n_o and (dn/dc) are the intercept and the slope of the solution refractive index concentration dependence, respectively, and λ is the laser wavelength.

Moreover, because of particle interactions it is expected that D_{app} depends on the scattering vector. A general expression for this diffusion coefficient is given by[10,51,52]

$$D_{app} = \frac{D_o[1 + H(q)]}{S(q)} \tag{11}$$

where $H(q)$ is the hydrodynamic function that accounts for the flow-related interactions and as $S(q)$ depends on the particle distribution in the sample, and D_o represents the diffusion coefficient at infinite dilution given by

$$D_o = \frac{kT}{6\pi\eta a_h} \tag{12}$$

with a_h and η representing the hydrodynamic radius of the diffusing particles and the medium viscosity, respectively. When, as in our case, the characteristic probing length of the scattering experiment $(2\pi/q)$ is much larger than the interparticle correlation length, the limit $q \to 0$ for the structure factor $(S(0))$ and the hydrodynamic function $(H(0))$ can be assumed in eqs 9 and 11, thus obtaining

$$D_{app} = D_o\frac{1 + H(0)}{S(0)} \tag{13}$$

$$\Delta R = cKMS(0) \tag{14}$$

The term $S(0)$ can be easily estimated as a limit of eq 7. Moreover, assuming pairwise additive hydrodynamic coupling, $H(0)$ can be calculated by using the following equation

$$H(0) = [\lambda_{fo} - \int_1^\infty F(x)[1 - g(x)]\,dx]\phi \tag{15}$$

For the terms of this equation, two satisfactory treatments obtained by Batchelor[53] and Felderhof[54] are available. The differences between the two treatments are very small, and the results obtained in the experimental data interpretation roughly agree within the estimated standard deviation (esd) values.[55] In this paper, we report the results obtained according to Felderhof treatment, which gives $\lambda_{fo} = -6.44$ and

$$F(x) = 12x - \frac{15}{8x^2} + \frac{27}{64x^4} + \frac{75}{64x^5} \tag{16}$$

The reported theory indicates that $g(x)$ is needed to exhaustively interpret static and dynamic scattering measurements. This function can be obtained by the solution of the Ornstein Zernike (OZ) equation for the net correlation function $h(x) = g(x) - 1$.[56] Depending on the particle interaction potential feature, different closure approximations can be used to solve this equation. In this paper we employed two of the most commonly used closures, which are the Percus Yevick (PY)[57] and the hypernetted chain (HNC). The PY closure is generally applied in cases of systems of particles interacting by means of just the excluded volume component, and we used it in the case of the HC model. The HNC is useful when the interaction potential consists of a hard-core plus a long-range part. The latter approximation was employed in the case of the EDL and the DLVO models. To solve the OZ equation under the HNC assumption an iterative procedure was followed.[10,58]

The above-mentioned relations constitute the fundamental principles for some of the most used procedures of SAXS data

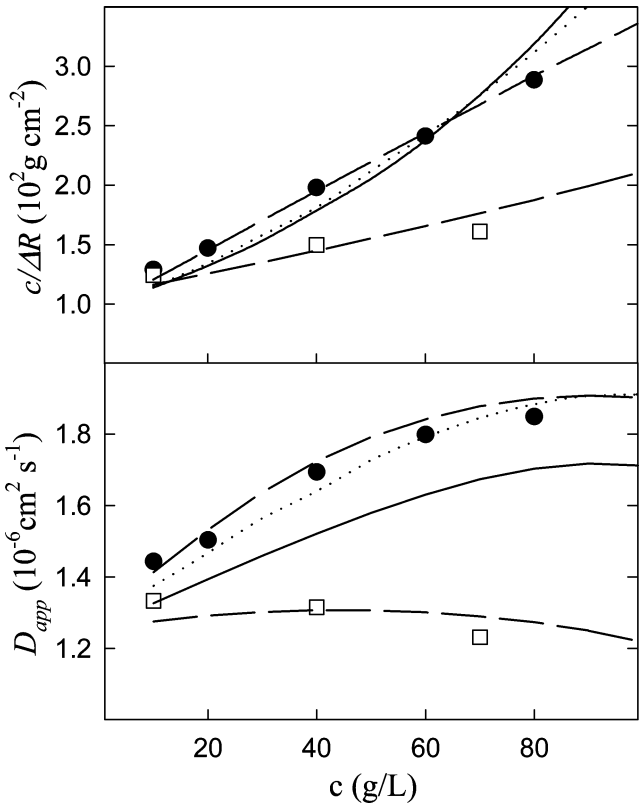

Figure 2. $c/\Delta R$ and D_{app} values of LY in 50 mM NaAc buffer (black circles) and in 50 mM NaAc buffer with 92 mM NaCl (open squares), as a function of the LY concentration. The curves represent the estimated patterns on the basis of the HC (full lines), EDL (dotted lines), and DLVO (dashed lines) models. The esd values are within the symbols.

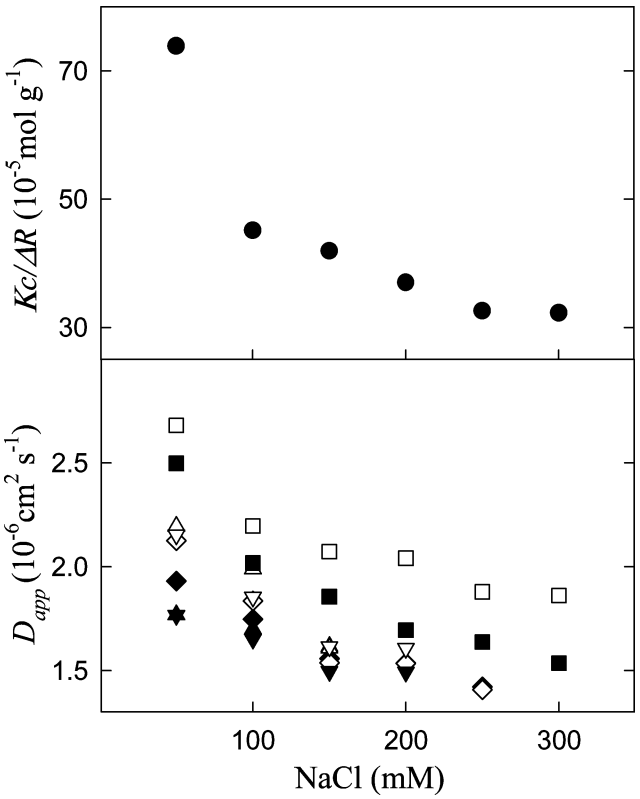

Figure 3. Experimental D_{app} (open squares) and $Kc/\Delta R$ values of 0.1 M NaGC aqueous solutions as a function of NaCl concentrations together with estimated D_{appc} values by assuming a spherical (up pointing triangles), an oblate (down pointing triangles), and a prolate (diamonds) symmetry on the basis of the HC (full symbols) and the EDL (open symbols) models. The D_{appc} values estimated on the basis of the DLVO model are also reported (full squares). The esd values are within the symbols.

interpretation. If a suitable guess of the interaction potential is available, then the SAXS spectra can be fitted by means of these procedures to obtain the geometrical parameters of the micelles and the $S(q)$ function. The basic principle of the comparative analysis reported in this paper is that the best fitting $S(0)$ values of the SAXS spectra can be used in eq 14 to interpret the SLS measurements. Moreover, an interpretation of the DLS data can be attempted. As a matter of fact, a hydrodynamic radius can be calculated from the SAXS best fitting particle geometrical parameters to estimate D_o (D_{oc}) by means of eq 12. Furthermore $g(x)$ obtained in terms of the extracted $S(q)$ Fourier transform as[59]

$$g(x) = 1 + \frac{4a^2}{12\pi\phi x}\int_0^\infty [S(q) - 1]q \sin(2qax)\,\mathrm{d}q \quad (17)$$

can be employed for the determination of $H(0)$ by means of eqs 15 and 16. This value together with the SAXS $S(0)$ and the D_{oc} values allows the estimation of a calculated D_{app} (D_{appc}). The comparison between D_{appc} and the experimental D_{app} provides some important information both on the colloidal particle features and on the validity of the interpretation methods.

Results and Discussion

Experimental Results. The DLS diffusion coefficient and the SLS $c/\Delta R$ ratio are reported for LY in 50 mM NaAc buffer, without added electrolyte and with 92 mM NaCl, as a function of the protein concentration (Figure 2). When non-self-assembling colloids are considered, the particle interaction effect on DLS and SLS data can be isolated by analyzing the slopes of D_{app} and $Kc/\Delta R$ vs c plots. In particular, for both of the data sets, a decrease of these slopes, in the dilute regime, is expected by decreasing the interaction potential repulsive character. If, as in our case, the term $c/\Delta R$ is reported to represent the SLS data, then the dependence on K of the experimental slope must be considered. However, only a very slight variation of n_o, dn/dc, and then of K values for LY solutions is expected in the studied NaCl concentration range. Therefore, the variation of the $c/\Delta R$ vs c plot slopes as a function of the NaCl molarity reflects essentially the added electrolyte dependence of the particle interaction effects on SLS data. In the case of charged particles that are characterized by an electrostatic component in the interaction potential, this means that SLS and DLS data trends can be significantly affected by the presence of an added electrolyte. On the basis of the DLVO potential, a general reason is that, as shown by the dependence on I of the electric double layer potential, a screening effect of the electrostatic component is expected by the ions in the medium. Sometimes, other effects, such as an electrolyte-induced variation of the particle charge because of ion binding or the onset of osmotic forces, are also invoked. The LY data confirm this behavior. Therefore a drastic lowering of the plot slopes in Figure 2 is observed when NaCl is added.

The SLS and DLS data are shown in Figure 3 for 0.1 M NaGC solutions as a function of NaCl molarity (0.05−0.30 M). In this case dn/dc measurements were performed. Within the experimental error the same value of 0.194 ± 0.001 mL g^{-1} was obtained for NaGC in 50 and 300 mM NaCl solution. By assuming this value and $n_o = 1.33$, K was estimated, and the scattering $Kc/\Delta R$ was reported. A typical trend of D_{app} values, very similar to that of the previously studied NaGC D_2O

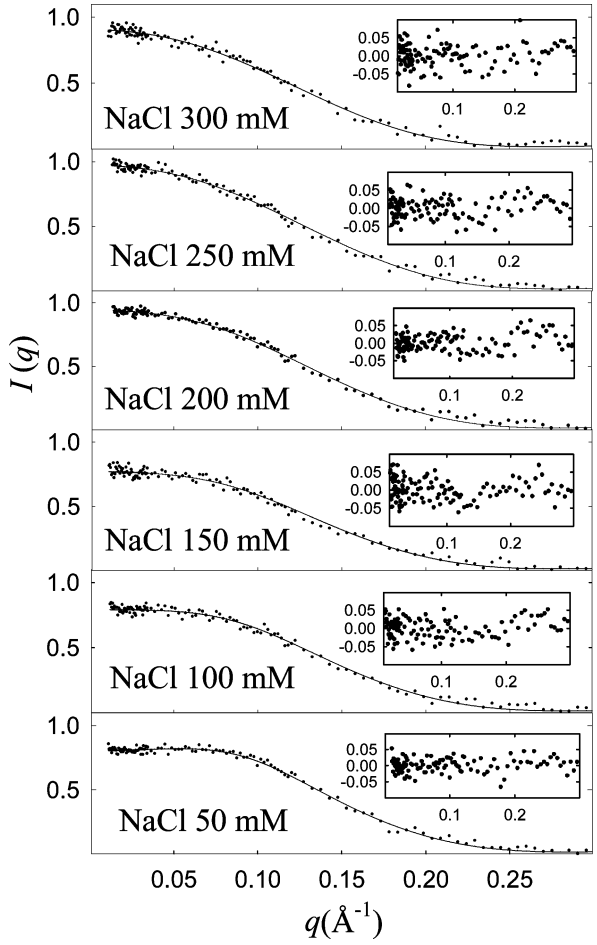

Figure 4. Smeared SAXS spectra of 0.1 M NaGC micellar solutions at different NaCl concentrations (dots). The solid lines are the theoretical fits assuming a spherical symmetry of the micelle and on the basis of the DLVO interaction model. The residuals are reported in the insets.

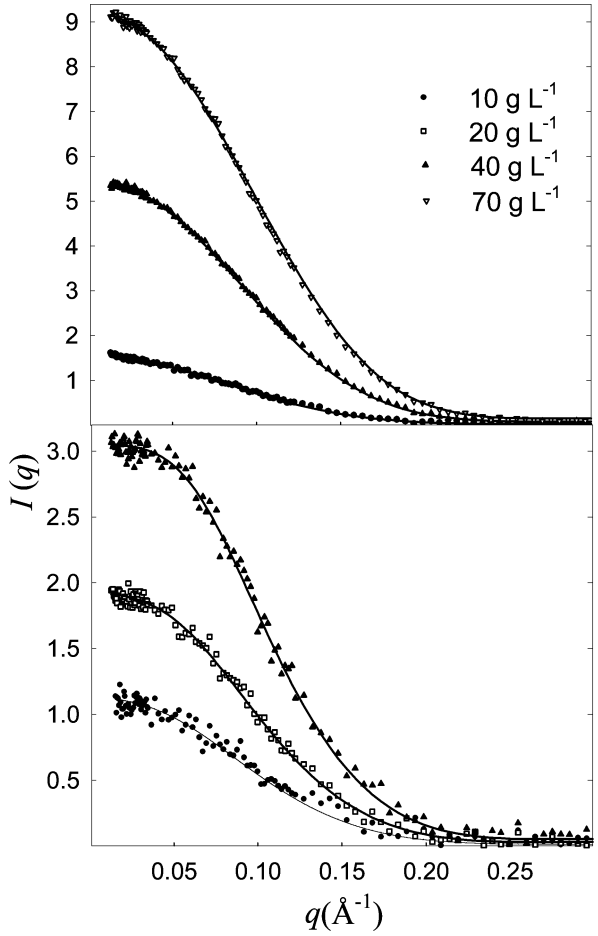

Figure 5. Experimental smeared SAXS spectra of LY in 50 mM NaAc buffer (lower panel) and 50 mM NaAc buffer with 92 mM NaCl (upper panel) (symbols). The solid lines are the calculated intensities for a prolate shape of the protein and the DLVO interaction model.

solutions, is observed (Figure 3).[18] In particular, large D_{app} values characterize the low ionic strength samples, where a strong electrostatic component dominates the intermicellar interaction potential. Therefore, the values gradually decrease by increasing the NaCl concentration, because of the progressive screening of the electrostatic repulsions. In agreement with this trend, a decrease of the scattering ratio with the NaCl concentration is observed.

SAXS spectra were recorded on the same NaGC solutions of Figure 3 and some of the LY solutions of Figure 2 (10−40 g L^{-1} LY in NaAc buffer and 10−70 g L^{-1} LY in NaAc buffer/NaCl solution). In the case of NaGC, the spectra very slightly change in the shape, mainly because of changes in the particle interaction potential, as a function of the NaCl concentration (Figure 4). The same effect is observed by comparing LY spectra at different electrolyte concentrations. Moreover, for the protein samples, an obvious increase of the $I(q)$ values and of the interaction effect is also observed in the spectra by increasing the LY concentration (Figure 5).

SAXS and SLS Data Interpretation. *LY.* It is well-known that the LY protein has a globular structure normally represented by a prolate ellipsoid;[60] therefore $F(q)$ for this geometry and the decoupling approximation (eq 8) was assumed in the SAXS fits. The known M of LY (14 600 Da) was used to estimate N_p and ϕ in the calculations (eqs 5 and 7), and the $\Delta\rho$ value for each sample was chosen as the best scale factor between SAXS calculated and experimental intensities. All the described models were used in the $S(q)$ estimation. For the EDL and DLVO representations, the buffer, the added NaCl, and the protein contribution were considered in the ionic strength calculation. Therefore, it was roughly estimated as $I = (c_{NaAc} + c_{NaCl} + {}^1/_2 c_{LY} Z)$, where c_{NaAc}, c_{NaCl}, and c_{LY} are the molar concentrations of NaAc, NaCl, and LY, respectively. Since no aggregation is expected for LY an overall fit of all the SAXS and SLS data was carried out by assuming the same particle semiaxes for all the samples.

As far as the DLVO model is concerned, the attractive interaction potential expressed in the Yukawa form with $J_{att} = -2.5\ kT$ and $d_{att} = 3$ Å was employed. This potential was proposed, for the first time, by Tardieu et al.[38] and successfully used in the interpretation of SAXS spectra of LY in conditions similar to those of our samples. In our minimization procedure, the J_{att} and d_{att} values were kept constant, and the ellipsoid semiaxes and Z were varied. Spherical particles with the same virial coefficient of the prolate ellipsoids were used in the $S(q)$ calculation.

It is well established that, when LY samples at different added electrolyte concentrations are studied assuming the DLVO model, the change of the ionic strength is not sufficient to explain the influence on the interaction potential induced by the electrolyte addition. On this subject, Tardieu et al. demonstrate that the assumption of a DLVO interaction potential with a NaCl-concentration-dependent Z value successfully accounts for the added electrolyte effect on SAXS spectra in a large range of NaCl molarities (0−350 mM). As a result, they obtained that Z is equal to 6.0 at low NaCl concentrations and gradually

TABLE 1: Best Fitting Parameters of the LY SAXS Spectra on the Basis of the HC, the EDL, and the DLVO Interaction Models (interaction potential parameters are *t* (HC model) and *Z* (EDL and DLVO models))[a]

			interaction potential parameter	
interaction model	a_e (Å)	b_e (Å)	0 mM NaCl	92 mM NaCl
HC	26.4	15.8	3.5	
EDL	26.5	15.7	5.5	
DLVO	27.0	15.6	7.7	6.9

[a] Estimated standard deviation values are within 1.5 Å (a_e), 0.5 Å (b_e), 0.2 Å (t), and 0.3 (Z).

decreases up to 2.1. However, a different approach was followed in a SAXS and light scattering study by Narayanan et al.[37] These authors, by starting from more general assumptions, employed the Tardieu et al. expression for the potential of mean force with a Yukawa attractive term accounting for both the van de Waals and the osmotic component. Therefore, they fit the data by assuming a constant value of $Z = 6$ at different added electrolyte concentrations. In this way, they obtained $J_{att} = -3kT$ and $d_{att} = 3$ Å at low NaCl molarity (8.6 mM), thus confirming the Tardieu et al. results. Conversely, at high NaCl concentrations (860 mM), they found a much lower value of J_{att} ($-10kT$) because of the onset of the osmotic attraction.

At our NaCl concentration, the effect of the osmotic contribution is very low, and the application of the Tardieu et al. or the Narayanan approaches is roughly equivalent. By following Tardieu et al., we performed an overall fit of all the LY data by assuming the same geometrical parameters for all the solutions and two different Z values at the two NaCl concentrations. The best fitting SAXS curves relative to the DLVO model are shown in Figure 5, and the corresponding parameters are reported in Table 1.

In the case of the HC model, the interaction shell thickness was varied together with the two semiaxes in the minimization procedure, and for each triplet of a_e, b_e, and t values the $S(q)$ function was estimated by applying the PY closure approximation[61,62] to the hard spheres with the same virial coefficient of the interaction ellipsoids (semiaxes $a_e + t$ and $b_e + t$). In the case of the EDL model as explained for the DLVO assumption, Z was varied together with the geometrical parameters.

Within the same NaCl concentration, the invariance of the interaction shell thickness t and of the charge Z was assumed in the HC and in the EDL models. Of course for the HC representation this means that the same interaction potential is considered for these samples. This assumption is quite drastic, since it does not account for the interaction potential dependence on the protein concentration that is related to the LY contribution to the ionic strength and therefore on the electrostatic interaction screening. However this contribution is quite low, and in view of the roughness of the model it was neglected.

It is worth mentioning that, since no attractive component is considered in the EDL representation, the best fitting Z values cannot be strictly related to the protein charge and must be considered just as a minimization parameter. For the same reason Z values lower than those obtained by assuming the DLVO potential are expected. Obviously, different t and Z values were considered for the samples with and without NaCl.

When the 92 mM NaCl spectra are fitted with the HC and EDL models, best fitting t and Z values equal to zero are obtained. This means that, on the basis of the static scattering data, the interaction potential tail is surely not repulsive in these conditions. Nothing more can be said on the features of this tail. However, we can suspect that the repulsive character that we assigned it could be a bad assumption for fitting the experimental data at these ionic strengths and probably the choice of an attractive tail could give rise to better fits. If so, then the best fitting parameters are conditioned by this forced assumption. Therefore, the overall fits with the HC and the EDL models were limited to the samples without NaCl. The best fitting curves are shown in Figure 6. The corresponding a_e, b_e, t, and Z values are reported in Table 1.

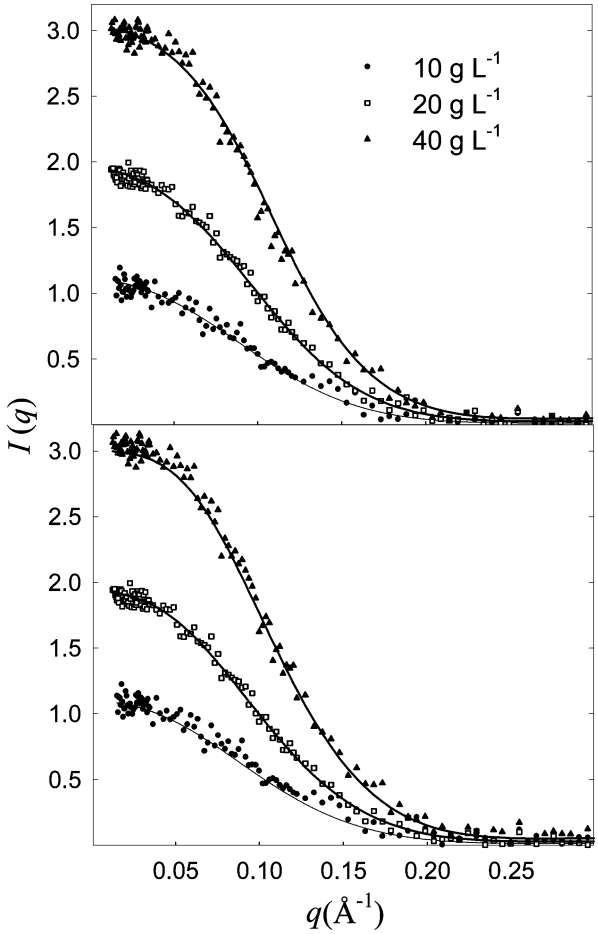

Figure 6. Experimental smeared SAXS spectra of LY in 50 mM NaAc buffer, at 25 °C (symbols). The solid lines are the theoretical fits assuming a prolate symmetry of the protein and on the basis of the HC (upper panel) and EDL (lower panel) interaction models.

To compare SAXS and SLS data, the $S(0)$ as a function of c was calculated for the scattering spectra best fitting parameters, with the $q \rightarrow 0$ form of eq 7. Therefore the $c/\Delta R$ ratio was estimated by means of eq 14. In this equation, the K value giving the best agreement between experimental and calculated scattering ratios was assumed. The obtained $c/\Delta R$ trends are reported in Figure 2. Very good consistency of the calculated curve and the experimental data is observed. From the best fitting K value, by assuming $n_o = 1.33$, the refraction index increment was calculated by means of eq 10. In the case of LY/NaAc buffer solutions, for all the used models, a best fitting K value is obtained corresponding to a dn/dc of 0.220 ± 0.003 mL g^{-1}. A slightly different best fitting dn/dc value of 0.216 ± 0.006 mL g^{-1} is given by the DLVO representation for the LY/NaCl/NaAc buffer samples. These values are in agreement with the data reported by Muschol and Rosenberger[63] for LY in similar mediums and for similar light wavelength (0.227 mL g^{-1}). This means that SAXS and SLS data can be successfully correlated in the mainframe of the employed interpretation models.

All the used models satisfactorily fit the SAXS spectra (Figures 5 and 6) and give very similar particle dimensions

(Table 1). The best fitting semiaxes are slightly greater than those obtained from the crystal structure,[64] thus indicating that the protein in solution is relatively less compact than in the crystal and/or is surrounded by a layer of structured hydration water molecules and ions having an electron density sensitively different from that of the bulk medium. If the gyration radii (R_g) are calculated from the best fitting semiaxes of Table 1, then very similar values with an average of 15.5 ± 0.3 Å are obtained, in agreement with values accepted in the literature and ranging from 14.3 to 15.5 Å.[65−67] The same semiaxes are slightly lower than the hydrodynamic ones reported by Dubin et al.[60] These differences are reasonable and are probably due to the choice of homogeneous particles to describe the LY scattering properties. In fact the results of Dubin et al. referred to a LY unsolvated molecule, roughly represented by a prolate ellipsoid with major and minor axes of 48 and 26 Å, covered with a shell of solvent about 3.5 Å thick. Very probably, this shell has an electron density relevantly different from that of the LY molecule and therefore is not properly accounted for if a homogeneous ellipsoid is used to fit the SAXS spectra.

Furthermore, a homogeneous sphere with a hydrodynamic radius of 18 Å has been used by Narayanan et al.[37] in their light scattering and SAXS study. This radius was assumed by considering an equivalent sphere of 17.2 Å for the unsolvated molecule and by allowing for a hydration layer thickness of 0.8 Å. The average of the hydrodynamic radii obtained from the dimensions of Table 1 by means of the Perrin equations[68] is equal to 19.1 ± 0.3 Å, which is greater than the value used by Narayanan et al. It must be said however that experimental hydrodynamic radii reported in the literature cover a large range of values (17.8−20.0 Å).[37,60,63,69] Therefore a definitive comparison between the sizes of our best fitting ellipsoid and the hydrodynamic sizes is not straightforward.

Detailed studies on the LY structure have been carried out by means of scattering measurements on dilute samples and in nonassociative conditions by Svergun et al.[66] Experimental SAXS and small-angle neutron scattering data of LY at different ionic strengths have been analyzed, and good agreements with the crystallographic structure have been pointed out. A fit improvement has been observed by assuming a 3-Å-thick hydration shell of bound water molecules with a density relative to the bulk solvent of 1.07−1.11.

A SAXS LY spectrum, collected in our laboratory, on a sample with a composition similar to one of those examined by Svergun et al. (LY 10 g L^{-1} in 0.15 M NaCl at pH 3.7), is shown in Figure 7.

An analysis performed with ITP[49] allowed us to determine the molecular weight and the R_g (14 600 Da and 14.8 Å, respectively). Moreover, the desmeared intensity was fit with the scattering curve calculated from the crystallographic structure by means of the CRYSOL program, and the smeared calculated curve is shown in Figure 7. The best fitting R_g, volume, and electron density contrast of the hydration shell are 14.9 Å, 18 500 $Å^3$, and 0.007 electrons $Å^{-3}$, respectively.

To test the consistency of our results, a fit of the experimental curve assuming $S(q) = 1$ and a homogeneous prolate ellipsoid model was carried out. The best fit, shown in Figure 7, was given by an ellipsoid with semiaxes 25.8 ± 0.5 Å, 14.8 ± 0.3 Å (R_g = 14.8 Å), and an electronic density contrast of 0.078 ± 0.004 electrons $Å^{-3}$. These results are roughly in agreement with those of Krigbaum et al. that for samples similar to that of Figure 7 and under the same interpretation mainframe obtained 25 and 14 Å as particle semiaxes and R_g = 14.3 Å. These semiaxes are sensitively lower than those reported in Table 1. However, since the latter were determined by extending the data interpretation to samples of interacting particles ($S(q) \neq 1$) and then by using a different interpretation approach, these differences are not astonishing.

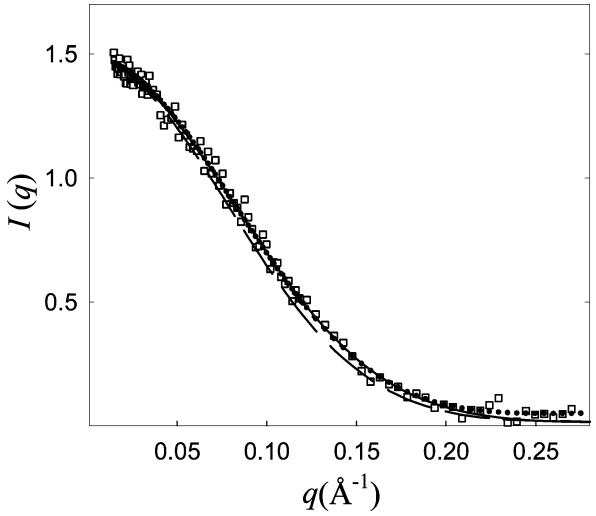

Figure 7. Experimental smeared SAXS spectrum of LY in 150 mM NaCl (open squares) together with the calculated curves obtained by using the CRYSOL program (dotted line), the best fitting homogeneous prolate ellipsoid (full line), and the DLVO ellipsoid of Table 1 (dashed line).

To further the result consistency analysis, the curve calculated by assuming the DLVO best fitting ellipsoid of Table 1 as scattering particle and $S(q) = 1$ was reported in Figure 7. Obviously, the curves are not perfectly superimposed; however they are roughly similar on an absolute scale, thus indicating that our $\Delta\rho$ value (0.068 ± 0.007 electrons $Å^{-3}$) and geometrical parameters are consistent with both the best fitting homogeneous ellipsoid and the more detailed and realistic model of ref 66.

The Z values derived from the DLVO treatment (Table 1) roughly agree with the results obtained, in similar conditions, by Tardieu et al.[38] and Narayanan et al.[37] (Z = 6.0) that, as previously mentioned, used the same parametrization of the interaction potential. However, quite different Z values have been reported by Muschol and Rosenberger[63] on the basis of SLS (10.7−10.9) and DLS (8.5−8.6) measurements, by assuming the DLVO interaction potential with the Hamaker expression (eq 4) for the attractive contribution with a steric protection thickness of 1.8 Å. Conversely, with a similar treatment, Z = 6.4 has been given by Eberstein et al.[70] by a DLS study on LY samples of widely varying concentrations in the presence of NaCl at pH = 4.2.

NaGC. In the case of the NaGC solutions, as whenever micellar systems are studied, the estimate for the micellar mass or aggregation number that strongly affects the SAXS intensity profile is often unavailable. If a reliable monomer molecular volume is known, then $\Delta\rho$ can be calculated during the fitting procedure, and M can be inferred as a fitting parameter of the SAXS spectra. However, since SLS measurements bring information on the molecular weight as well (eqs 9 and 14), the monomer molecular volume is not needed in our case, and a correlated interpretation of SAXS and SLS data can be performed to obtain both the M and $\Delta\rho$ values. Because K is easily determinable by means of refractive index measurements, SLS experiments represent one of the most common and reliable ways to determine the colloidal particle molar mass. Generally, the extrapolation method is used, and M is evaluated, by means of eq 14, from the $Kc/\Delta R$ value extrapolated to infinite dilution, for which $S(0) = 1$ is assumed. This procedure could be

followed in the case of LY solution since no aggregation is expected in the studied conditions. Actually, for micellar solutions, the extrapolation should be avoided and $S(0)$ should be estimated for each sample. As described in the theoretical background section, the SAXS best fitting $S(0)$ can be used to this aim. However, as stated in the same section, there is a strict dependence between the SAXS $I(q)$ and the M value, and therefore an overall fit of SAXS and SLS data is needed. In this work, this fit was carried out by systematically varying the interaction potential and geometrical parameters and by calculating the $I(q)$ SAXS curves with the best fitting M value of the experimental $Kc/\Delta R$. To this aim, for each set of geometrical and potential parameters $S(0)$ was estimated by systematically varying M up to the couple of M and $S(0)$ values that give the best agreement with the SLS data. For each M value, the aggregation number was calculated as $n_{agg} = M/M_{NaGC}$, and the micellar charge number was estimated as $Z = n_{agg}\alpha$, where α is the ionization degree. In the calculations, the micelle concentration was expressed as $c = c_T - \text{cmc}$, where c_T and cmc are the NaGC total and critical micellar weight/volume concentrations. The ionic strength was calculated as $I = (\text{cmc}_M + c_{NaCl}) + 1/2\alpha(c_M - \text{cmc}_M)$, where cmc_M and c_M are the NaGC total and the critical micellar molarities.[19] Even in this case, the $\Delta\rho$ value was determined as the best scale factor between SAXS calculated and experimental intensities.

It is known that NaGC gives rise to small micelles that very slightly grow by increasing the NaCl concentration. For this reason, as a first approach, the simple model of homogeneous and spherical particles was assumed in the interpretation.

In the cases of the HC and EDL models, the micellar radius a and t or α were varied, and each sample was singly fitted. The best fitting curves are reported in Figure 8, and the corresponding parameters are listed in Table 2. As mentioned above, the HC and EDL results have a physical meaning only when the repulsion dominates the potential tail. For this reason only the parameters corresponding to fits that give t and α greater than zero are reported.

Several published results show that, because of their peculiar amphiphilic structure (Figure 1), the bile salts could give rise to slightly anisotropic-shaped micelles even at low aggregation numbers. Therefore, to account for the eventually anisotropic shape of the NaGC micelles, homogeneous ellipsoidal particles were also employed to represent the aggregates in the interpretation of the SAXS spectra. However, both oblate and prolate ellipsoids were tried, and no significant differences were pointed out between the fits with the two symmetries, which both give an excellent agreement between calculated and experimental intensities. The best fitting curves (for t and $\alpha > 0$) are reported in Figures 9 and 10. With respect to the spherical case, marked improvements of the SAXS fits are observed with both the ellipsoidal shapes. In any case, the residual patterns for the two micelle geometries are very similar, thus rendering impossible the choice of the best shape to describe the NaGC aggregates. The best fitting SAXS parameters obtained with this treatment are reported in Table 3.

An inspection of Tables 2 and 3 shows that comparable particle geometrical parameters are given by the HC or the EDL interaction models. Both the sizes and the aggregation numbers indicate that the micelles only very slightly grow by increasing the added electrolyte concentration. The t values point out that the electrostatic interactions sensitively affect the SAXS pattern at low NaCl concentrations. However, these interactions are rapidly screened by increasing the electrolyte molarity. If the EDL model is used, then a decrease of α is observed because of the NaCl addition. Actually, as already mentioned, since the EDL potential gives an incomplete definition of the intermicellar potential tail, the physical meaning of α deserves more discussion. In fact, when micellar systems are studied it is normally assumed that the micelle ionization degree does not depend on the added electrolyte concentration. This hypothesis can be verified if both the van der Waals attractive and the electrostatic repulsive components of the potential tail are taken into account.[18] Conversely, if only the electrostatic component is used to approximate the tail, then an unrealistic lowering of α is needed to balance the missing attractive component. This means that the α value at 50 mM NaCl, which is the lowest of our added electrolyte concentrations, is also the more realistic one, since for this sample the electrostatic repulsion largely

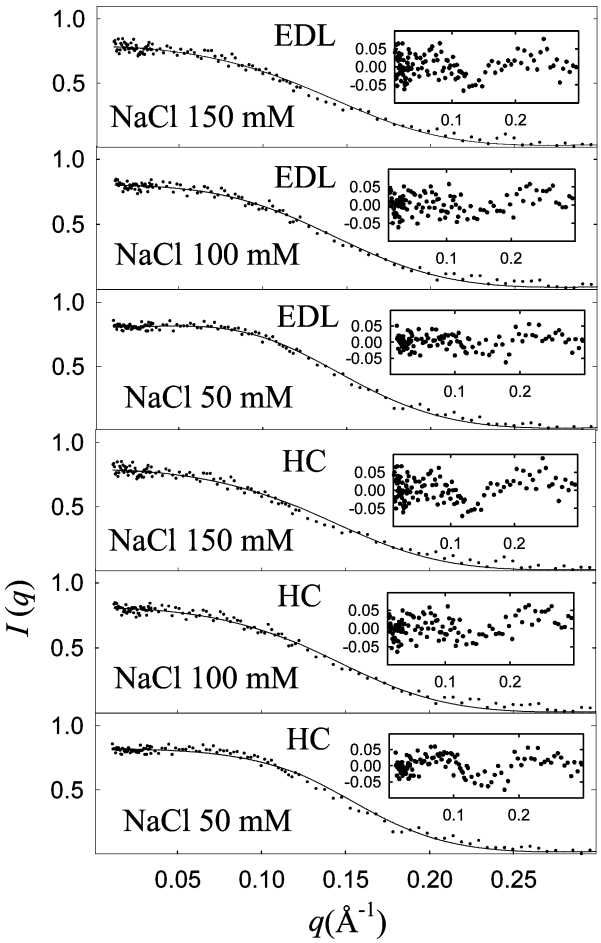

Figure 8. Smeared SAXS spectra of 0.1 M NaGC micellar solutions at different NaCl concentrations (dots). The solid lines are the theoretical fits assuming a spherical symmetry of the micelle and on the basis of the HC (HC panels) and EDL (EDL panels) interaction models. The residuals are reported in the insets.

TABLE 2: Best Fitting Micellar a (Å), t (Å), α, n_{agg}, n_{aq}, and $\Delta\rho$ (electrons Å^{-3}) of SAXS Spectra and SLS Data as a Function of NaCl Concentration on the Basis of the HC and the EDL Interaction Models, by Assuming a Spherical Shape for the Micelles[a]

	HC model				EDL model				
NaCl (mM)	a	t	n_{agg}	$\Delta\rho$	a	α	n_{agg}	$\Delta\rho$	n_{aq}
50	15.4	1.3	7.7	0.028	15.4	0.59	8.7	0.029	38
100	15.4	0.6	9.4	0.029	15.4	0.38	9.9	0.029	30
150	15.7	0.1	9.6	0.027	15.7	0.06	9.6	0.027	35

[a] Estimated standard deviation values are within 0.2 Å (a and t), 0.02 (α), 0.3 (n_{agg}), 3 (n_{aq}), and 0.001 electrons Å^{-3} ($\Delta\rho$).

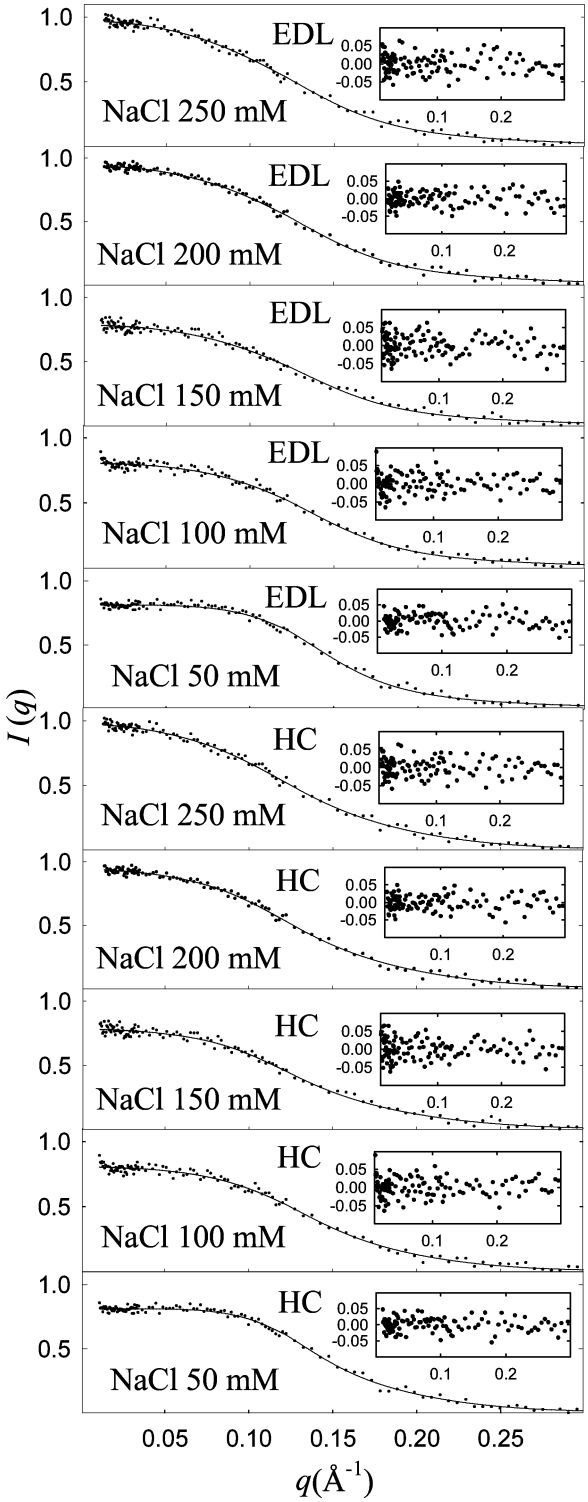

Figure 9. Smeared SAXS spectra of 0.1 M NaGC micellar solutions at different NaCl concentrations (dots). The solid lines are the theoretical fits assuming a prolate symmetry of the micelle and on the basis of the HC (HC panels) and EDL (EDL panels) interaction models. The residuals are reported in the insets.

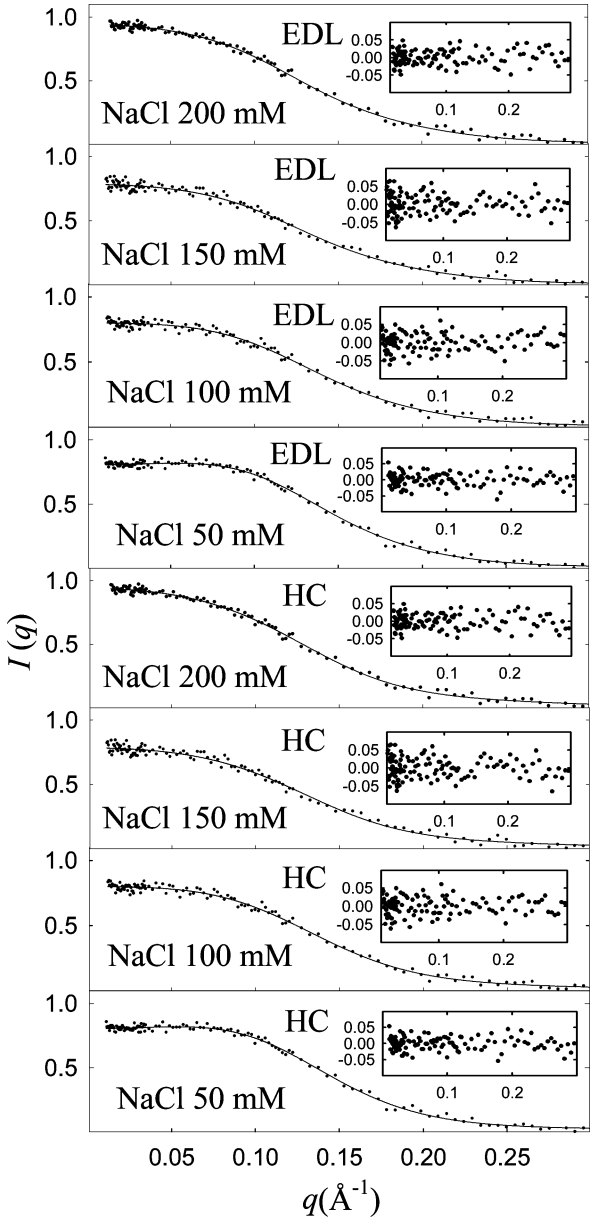

Figure 10. Smeared SAXS spectra of 0.1 M NaGC micellar solutions at different NaCl concentrations (dots). The solid lines are the theoretical fits assuming an oblate symmetry of the micelle and on the basis of the HC (HC panels) and EDL (EDL panels) interaction models. The residuals are reported in the insets.

prevails on the attractive component and the EDL model more reliably describes the particle interaction potential.

As shown in Tables 2 and 3, very similar $\Delta\rho$ values were obtained for all the studied samples with both of the interpretation models and all of the assumed geometries. Of course these parameters are strictly related to the micellar structure and can be used to further characterize the aggregates. If only the glycocholate anion (GC^-), the bounded counterions (Na^+), and some water molecules are supposed to be present inside the micelles, then $\Delta\rho$ can be roughly expressed as

$$\Delta\rho = \frac{n_{agg}e_{GC} + (1-\alpha)n_{agg}e_{Na} + n_{agg}n_{aq}e_{aq}}{V_m} - \rho_s \quad (18)$$

where e_{GC}, e_{Na}, and e_{aq} are the number of electrons of GC^-, Na^+, and the water molecule, respectively, n_{aq} is the number of water molecules per monomer in the micelle, V_m is the micellar volume, and ρ_s is the medium electronic density. Obviously, the number of electrons for each species is known. Moreover, as $\Delta\rho$, the n_{agg}, α, and V_m values are obtained as the best fitting SAXS parameters. This means that, if the ρ_s value is estimated for each sample, then the hydration number of the micelles can be calculated. With this procedure, the n_{aq} values were determined (Tables 2 and 3). Because of the previous discussion the α value corresponding to the 50 mM NaCl sample was used

TABLE 3: Best Fitting a_e (Å), b_e (Å), t (Å), α, n_{agg}, n_{aq}, and Δρ (electrons Å^{-3}) Values of SAXS Spectra Obtained by Assuming Prolate and Oblate Ellipsoidal Shape of the Micelles on the Basis of the HC and the EDL Interaction Models as a Function of the NaCl Concentration (mM)[a]

		HC Model					EDL Model					
	NaCl	a_e	b_e	t	n_{agg}	Δρ	a_e	b_e	α	n_{agg}	Δρ	n_{aq}
oblate	50	20.7	9.6	2.4	9.7	0.030	19.1	10.4	0.65	9.6	0.031	34
	100	20.7	9.3	1.5	11.3	0.031	20.0	9.6	0.49	11.3	0.032	26
	150	21.5	9.3	0.5	11.4	0.029	21.1	9.5	0.39	11.7	0.029	29
	200	21.6	9.3	0.5	12.2	0.032	21.4	9.3	0.40	12.4	0.032	27
prolate	50	31.9	12.1	2.5	10.9	0.030	24.2	12.7	0.67	9.9	0.031	35
	100	31.7	12.0	1.7	12.6	0.030	26.6	12.4	0.51	11.8	0.031	27
	150	42.3	11.8	1.0	15.3	0.028	33.9	12.2	0.45	13.3	0.028	32
	200	42.1	11.7	0.9	16.0	0.031	35.0	12.2	0.49	14.6	0.031	29
	250	42.1	11.9	0.2	16.4	0.031	37.6	12.2	0.24	15.1	0.030	31

[a] Estimated standard deviation values are within 0.3 Å (a_e, b_e, and t), 0.02 (α), 0.3 (n_{agg}), 3 (n_{aq}), and 0.001 electrons Å^{-3} (Δρ).

in the calculations. It is important to remark, that the assumed composition for the micelle is probably drastic, since the hypothesis that Na^+ and Cl^- ions are coordinated to the hydration water molecules cannot be discarded. However, even if NaCl with the same concentration of the bulk is supposed to be dissolved in the hydration water, no relevant variation in the n_{aq} values is observed. In any case, from these results, by considering the reasonable volumes of 30 and 14.1 Å^3 for a water molecule (V_{aq}) and a Na^+ cation (V_{Na}) (corresponding to a Na^+ radius of 1.5 Å), respectively, a GC^- anion volume can be estimated as $V_{GC} = V_{nGC}/n_{agg}$ where $V_{nGC} = V_m - n_{agg}(1 - \alpha)V_{Na} - n_{agg}n_{aq}V_{aq}$. In this way, very similar values are obtained with all of the assumed geometries, with an average of 617 ± 20 Å^3. Despite the drastic assumptions that we have made in the calculation, this value is in very good agreement with data reported in the literature for NaGC (∼600 Å^3),[71] thus supporting the overall consistency of the data analysis. Obviously, because of the drastic assumption of particle homogeneity, the n_{aq} values must be considered a rough estimation of the micelle hydration. However they clearly indicate that the micelles are relevantly hydrated.

The similarity between geometrical parameters and Δρ values obtained with the HC and the EDL representations from the NaGC data demonstrates that the static scattering data interpretation is very poorly affected by the details of the interaction potential. This conclusion is confirmed by the LY results where this similarity is extended to the DLVO model also. This means that, despite the roughness of the interaction models, the NaGC structural results are very probably reliable. However, to reliably define the NaGC micelle interaction potential, the complete DLVO model must be used. Actually, the number of parameters defining the DLVO potential does not allow an unequivocal interpretation of the SAXS spectra. Fortunately, in view of the previous discussed results some reasonable constraints can be assumed for the interaction potential parameters in different NaGC samples. The first constraint, which is based on the above-mentioned common assumption in the micelle behavior interpretation, is that the micelle α value is not affected by the added electrolyte; the second assumption concerns the Hamaker constant. With variance of the NaCl concentration, this constant can change both for the direct variation of the medium composition and for the induced changes in the composition of the micelles.[72] However, in the studied NaCl concentration range the medium contribution should be negligible, and the micelle composition does not seem to change relevantly. In fact this variation should be essentially determined by changes of the monomer density in the aggregate that, in our interpretation, should be accompanied by a variation of the Δρ or n_{aq} values. Actually, these terms, even if sensitively fluctuating around their average value, do not seem to show any systematic dependence on the NaCl concentration. Hence, the Hamaker constant can be reasonably considered invariant in all the studied samples. Of course, this means that the same J_{att} and d_{att} values well describe the attractive potential in all the solutions, if the Yukawa form is chosen.

TABLE 4: Best Fitting a (Å) Values of SAXS Spectra Obtained by Assuming a Spherical Shape of the Micelles on the Basis of the DLVO Interaction Model as a Function of the NaCl Concentration (mM)

NaCl	50	100	150	200	250	300
a	15.0	15.1	15.4	15.4	15.5	16.0

In view of all these considerations, an overall fit of all the NaGC/NaCl solutions was attempted by means of the DLVO model in which constant α, J_{att}, and d_{att} were assumed. For sake of simplicity just the spherical case was considered, and an iterative procedure was followed. In the first step, the 300 mM NaCl scattering data were fitted by assuming the EDL best fitting α value of the 50 mM NaCl solution as a known parameter, thus considering the micellar radius and the J_{att} and d_{att} values as fitting variables. Afterward, these best fitting values were fixed, and the fit of the 50 mM NaCl data was performed by varying the α and a values. To perform the iteration, the fits of the two spectra were alternatively repeated, by alternatively fixing the attractive and the repulsive interaction parameters, up to convergence.

The best overall fit of the two solutions is obtained with α = 0.82 ± 0.03, $J_{att} = -3.8kT$, and $d_{att} = 1.4$ Å. However, in the minimization we observe that the latter two parameters are strictly correlated and satisfactory agreements are obtained with different couples of values within the ranges $-3.5kT > J > -4.1kT$ and $1.2 < d < 1.6$ Å. Moreover, by means of eq 18 very similar n_{aq} values equal to ∼35 are estimated for the two samples. With α, J_{att}, and d_{att} fixed at their best fitting values, the other spectra were fit by changing just the particle radius a. Moreover, to guarantee the invariance of the monomer density in the micelles, $n_{aq} = 35$ was imposed as a further constraint. The best fitting curves together with the experimental patterns are shown in Figure 4, and the corresponding a values are reported in Table 4.

Satisfactory fits are obtained, thus indicating that the slight micelle growth and the screening effect on the electrostatic interactions, because of the ionic strength increase, are sufficient to explain the added electrolyte influence on the NaGC micelle system.

DLS Data Interpretation. From the best fitting set of parameters of the scattering data the D_{appc} was calculated as reported in the Theoretical Background section. In the calculation, a_h equal to the best fitting a value of each sample was used in eq 12 to estimate D_{oc} under the assumption of spherical

NaGC micelles. For LY and NaGC ellipsoidal micelles, the same equation with the equivalent hydrodynamic radii for prolate or oblate ellipsoids, derived from the best fitting semiaxis values by Perrin equations,[68] was used. Moreover, in view of the not very high anisotropy presented by the best fitting ellipsoids, the hydrodynamic interactions were treated as for spherical particles, thus preserving the form of eqs 11 and 12. The estimated D_{appc} values are reported for each single NaGC sample in Figure 3 and as a D_{appc} versus c curve for LY in Figure 2.

As shown in Figure 2 (lower panel), the agreement between the D_{appc} curves and the experimental points improves sensitively by changing the interaction model in the order HC → EDL → DLVO, namely, by using more refined and realistic potentials. On the average, the same improvement is observed in the case of NaGC for the consistency of the discrete D_{app} and D_{appc} values. It must be stressed, however, that whatever is the interaction representation used D_{appc} values systematically lower than the experimental D_{app} are obtained for the micellar solutions (Figure 3). This result was already observed in the correlation of NaTDC SAXS and DLS data.[15] However, it was not deeply discussed in that case since only the HC and EDL potentials were used whose roughness was supposed to affect the results. Actually, the present work indicates that this discrepancy cannot be ascribed to the interaction model. As a matter of fact, the comparison between the D_{appc} curves and the experimental points of Figure 2 indicates that the EDL model, when applicable (low ionic strength), gives consistent results for LY even at mass densities greater than that of NaGC (48.7 g L^{-1}). Moreover, even the assumption of a quite complete interaction potential, as the DLVO, which gives a satisfactory agreement for LY at both the ionic strengths (Figure 2), is not sufficient to close the gap between the two NaGC data sets. Therefore, other reasons must be invoked, for example, related to the assumptions on the structure of the micelles. As shown in Figure 3, no systematic improvements are observed by using the oblate or prolate ellipsoids to represent the micelles, thus indicating that the diffusivity data consistency is poorly affected by the imposed particle geometry. Beyond this factor, the choice of homogeneous aggregates could be responsible for the inconsistency between D_{app} and D_{appc}. Actually, the good results reported for the protein solution, under the same assumption, seem to show that this disagreement cannot be totally ascribed to the imposed homogeneity of the particles. Obviously this is true unless very drastic and peculiar inhomogeneities characterize the micelles.

By holding this possibility for the NaGC aggregates, we must remember, however, that the micelle polydispersity complicates the NaGC data analysis and could be invoked as a further reason to explain the differences between protein and micelle data agreements. This property can be accounted for in the static scattering data analysis, but unfortunately, an exhaustive theory for DLS on polydisperse systems is not available so far. It is important to remark, moreover, that in the case of micellar solutions the micelle dynamics, such as formation and destruction processes, can remarkably influence the sample scattered intensity fluctuations, thus further complicating the DLS data interpretation.

As a final comment on the diffusivity data it is important to remark that although the agreement between the calculated and the experimental D_{app} for LY is much better than that in the NaGC case it is still far from being excellent. Beyond the already discussed structural assumption, we must remember that the drastic approximation to pairwise hydrodynamic interactions for all the studied samples very probably affects the quality of our results. Further work is in progress to verify this hypothesis.

Conclusions

It is known that fits of SAXS spectra are poorly affected by the details of the interparticle potential. For this reason, when both particle structure and interactions are unknown, the SAXS patterns are generally fit by assuming very simple potential functions so as to minimize the number of fitting parameters. Depending on the experimental conditions, this leads, for example, to treatment of complex systems with simple repulsive or attractive functions describing the potential tail. For colloidal particles, the DLVO model is one of the best representations of this tail since it contains both the van der Waals attractive and the electrostatic repulsive components. Conversely, the HC and the EDL models are simplified approximations when the repulsive contribution dominates. Obviously, when applied to the interpretation of SAXS data, the latter allow a satisfactory definition of the particle structure but an unrealistic description of the interparticle potential. On the contrary, satisfactory descriptions of the interactions on the basis of the DLVO model are provided by SLS and DLS studies based on the extrapolation method. This method, however, is not reliable for micellar systems.

This paper reports a SAXS, SLS, and DLS data correlation, based on the above-mentioned interaction models, as a tool for characterizing structure and interactions of colloidal particles without resorting to extrapolation procedures. This correlation was first tested on LY solutions and then used to study NaGC micelles.

In the case of LY, whose structure and interaction potential have been widely studied in the literature, all the models were easily applied. In particular, the interpretation with the DLVO representation was possible by assuming the attractive component as a known term to limit the number of fitting parameters. The results show that the correlation of the techniques improves by changing the models in the order HC → EDL → DLVO, namely, by using more refined and realistic potential, thus indicating that the proposed approach represents a valuable tool for investigating the particle interaction. Moreover, in the DLVO case, a good agreement with data reported in the literature is pointed out, which is testament of the validity of our correlation.

Concerning the NaGC micelles, for which very few data are published, all of the parameters of both structure and interaction potential were always assumed unknown. Therefore, from the SAXS and SLS data interpretation on the basis of the rough HC and EDL models, a satisfactory description of the micelles in terms of size, aggregation number, and hydration was achieved. Beyond this classical approach, an unusual overall fit of SAXS and SLS measurements on NaGC aqueous solutions at different NaCl concentrations was performed by assuming the complete DLVO model, thus providing more reliable definitions of both micelle structure and intermicellar potential. Satisfactory fits were obtained by imposing the same ionization degree and attractive component of the interaction potential at all the NaCl molarities, thus showing that the influence on the micelle size and on the medium ionic strength justifies the added NaCl effect. It is important to remark that, by using the SLS data, these results were obtained without any previous assumption on the NaGC molecular volume. In fact, this term, which is necessary to fit SAXS spectra alone on an absolute scale, was obtained as a further best fitting parameter of a SAXS−SLS simultaneous minimization.

The consistency between calculated and experimental DLS data confirms the dependence on the interaction potential

representations observed for LY. However, unlike the LY case, calculated apparent diffusion coefficients systematically lower than the experimental ones are obtained, even with the best potential model (DLVO). This result leads to an important consideration, namely, that it could be misleading to approximate the micelles by rigid objects moving inside the solution. In fact a micelle internal dynamic involving, for example, formation and destruction processes, which could significantly affect the DLS experiments, must be taken into account. It must be stressed however that the micelle polydispersity, which could also affect the data consistency, was not accounted for in our analysis. Unfortunately, this was a forced choice since an exhaustive theory for DLS on systems of polydisperse and interacting particles is not available so far.

Acknowledgment. Thanks to Professor Giuseppe Briganti for the refractive index measurements and to Professor Edoardo Giglio for valuable discussions. This work was sponsored by Italian Ministero dell'Istruzione, dell'Università e della Ricerca (Cofin N*o*. 20020371541).

References and Notes

(1) Bendedouch, D.; Chen, S.-H.; Koehler, W. C. *J. Phys. Chem.* **1983**, *87*, 2621.
(2) Bendedouch, D.; Chen, S.-H. *J. Phys. Chem.* **1984**, *88*, 648.
(3) Bendedouch, D.; Chen, S.-H. *J. Phys. Chem.* **1983**, *87*, 1653.
(4) Kotlarchyk, M.; Chen, S.-H. *J. Chem. Phys.* **1983**, *79*, 2461.
(5) Dorshow, R.; Briggs, J.; Bunton, C. A.; Nicoli, D. F. *J. Phys. Chem.* **1982**, *86*, 2388.
(6) Dorshow, R. B.; Bunton, C. A.; Nicoli, D. F. *J. Phys. Chem.* **1983**, *87*, 1409.
(7) Imae, T. *J. Phys. Chem.* **1988**, *92*, 5721.
(8) Tracy, M. A.; Pecora, R. *Macromolecules* **1992**, *25*, 337.
(9) Corti, M.; Degiorgio, V. *J. Phys. Chem.* **1981**, *85*, 711.
(10) Ortega, F.; Bacaloglu, R.; McKenzie, D. C.; Bunton, C. A.; Nicoli, D. F. *J. Phys. Chem. B* **1990**, *94*, 501.
(11) Janich, M.; Lange, J.; Graener, H.; Neubert, R. *J. Phys. Chem. B* **1998**, *102*, 5957.
(12) Missel, P. J.; Mazer, N. A.; Benedek, G. B.; Young, C. Y.; Carey, M. C. *J. Phys. Chem.* **1980**, *84*, 1044.
(13) Porte, G.; Appel, J. *J. Phys. Chem.* **1982**, *85*, 2511.
(14) Galantini, L.; Giglio, E.; Leonelli, A.; Pavel, N. V. *J. Phys. Chem. B* **2004**, *108*, 3078.
(15) Cozzolino, S.; Galantini, L.; Leggio, C.; Pavel, N. V. *J. Phys. Chem. B* **2005**, *109*, 6111.
(16) D'Archivio, A. A.; Galantini, L.; Tettamanti, E. *J. Phys. Chem. B* **2000**, *104*, 9255.
(17) Galantini, L.; Pavel, N. V. *J. Chem. Phys.* **2003**, *118*, 2865.
(18) Galantini, L.; Giampaolo, S. M.; Mannina, L.; Pavel, N. V.; Viel, S. *J. Phys. Chem. B* **2004**, *108*, 4799.
(19) Galantini, L.; Giglio, E.; Pavel, N. V.; Punzo, F. *Langmuir* **2003**, *19*, 1319.
(20) D'Alagni, M.; D'Archivio, A. A.; Galantini, L.; Giglio, E. *Langmuir* **1997**, *13*, 5811.
(21) Bonincontro, A.; Briganti, G.; D'Archivio, A. A.; Galantini, L.; Giglio, E. *J. Phys. Chem. B* **1997**, *101*, 10303.
(22) Bonincontro, A.; D'Archivio, A. A.; Galantini, L.; Giglio, E.; Punzo, F. *J. Phys. Chem. B* **1999**, *103*, 4986.
(23) Mazer, N. A.; Carey, M. C.; Kwasnick, R. F.; Benedek, G. B. *Biochemistry* **1979**, *18*, 3064.
(24) Schurtenberger, P.; Mazer, N.; Känzig, W. *J. Phys. Chem.* **1983**, *87*, 308.
(25) Esposito, G.; Giglio, E.; Pavel, N. V.; Zanobi, A. *J. Phys. Chem.* **1987**, *91*, 356.
(26) Jover, A.; Meijide, F.; Rodrýguez Núñez, E.; Vázquez Tato, J. *Langmuir* **1996**, *12*, 1789.
(27) Funasaki, N.; Fukuba, M.; Kitagawa, T.; Nomura, M.; Ishikawa, S.; Hirota, S.; Neya, S. *J. Phys. Chem. B* **2004**, *108*, 438.
(28) Bottari, E.; D'Archivio, A. A.; Festa, M. R.; Galantini, L.; Giglio, E. *Langmuir* **1999**, *15*, 2996.
(29) Stabinger, H.; Kratky, O. *Makromol. Chem.* **1978**, *179*, 1655.
(30) *Small Angle X-ray Scattering*, Glatter, O., Kratky, O., Eds.; Academic Press: London, 1982.
(31) Orthaber, D.; Bergmann, A.; Glatter, O. *J. Appl. Crystallogr.* **2000**, *33*, 218.
(32) Glatter O. *J. Appl. Crystallogr.* **1974**, *7*, 147.
(33) Siegert, A. J. F. *MIT Radiation Laboratory Report No. 465*; Massachusetts Institute of Technology: Cambridge, MA, 1943.
(34) Koppel, D. E. *J. Chem. Phys.* **1972**, *57*, 4814.
(35) Verwey, E. J. W.; Overbeck, J. Th. G. *Theory of the Stability of Lyophobic Colloids*; Elsevier: New York, 1948.
(36) Hamaker, H. C. *Physica* **1937**, *4*, 1058.
(37) Narayanan, J.; Liu, X. Y. *Biophys. J.* **2003**, *84*, 523.
(38) Tardieu, A.; Le Verge, A.; Malfois, M.; Bonneté, F.; Finet, S.; Riés-Kautt, M.; Belloni, L. *J. Cryst. Growth* **1999**, *196*, 193.
(39) Curtis, R. A.; Prausnitz, J. M.; Blanch, H. W. *Biotechnol. Bioeng.* **1998**, *57*, 11.
(40) Alami, E.; Abrahmsén-Alami, S.; Eastoe, J.; Heenan, R. K. *Langmuir* **2003**, *19*, 18.
(41) Hjelm, R. P.; Schteingart, C. D.; Hofmann, A. F.; Thiyagarajan, P. *J. Phys. Chem. B* **2000**, *104*, 197.
(42) Lusvardi, K. M.; Full, A. P.; Kaler, E. W. *Langmuir* **1995**, *11*, 487.
(43) Weber, V.; Narayanan, T.; Mendes, E.; Schosseler, F. *Langmuir* **2003**, *19*, 992.
(44) Haldar, J.; Aswal, V. K.; Goyal, P. S.; Bhattacharya, S. *J. Phys. Chem. B* **2004**, *108*, 11406.
(45) Mangiapia, G.; Berti, D.; Baglioni, P.; Teixeira, J.; Paduano, L. *J. Phys. Chem. B* **2004**, *108*, 9772.
(46) Caponetti, E.; Chillura-Martino, D.; Pedone, L. *Langmuir* **2004**, *20*, 3854.
(47) Liu, H.; Skibinska, L.; Gapinski, J.; Patkowski, A.; Fischer, E. W.; Pecora, R. *J. Chem. Phys.* **1998**, *109*, 7556.
(48) Cichocki, B.; Felderhof, B. U. *J. Chem. Phys.* **1991**, *94*, 556.
(49) Glatter, O. *J. Appl. Crystallogr.* **1977**, *10*, 415.
(50) Svergun, D. I.; Barberato, C.; Koch, M. H. J. *J. Appl. Crystallogr.* **1995**, *28*, 768.
(51) Pusey, P. N.; Tough, R. J. A. In *Dynamic Light Scattering*; Pecora, R., Ed.; Plenum: New York, 1985; Chapter 4.
(52) Dhont, J. K. G. *An Introduction to Dynamics of Colloids*; Möbius, D., Miller, R., Eds.; Elsevier: Amsterdam, 1996.
(53) Batchelor, G. K. *J. Fluid. Mech.* **1976**, *74*, 1.
(54) Felderhof, B. U. *J. Phys. A* **1978**, *11*, 929.
(55) Venkatesan, M.; Hirtzel, C. S.; Rajagopalan, R. *J. Chem. Phys.* **1985**, *82*, 5685.
(56) Ornstein, L. S.; Zernicke, F. *Proc. Akad. Sci.* **1914**, *17*, 793.
(57) Percus, J. K.; Yevick, G. *J. Phys. Rev.* **1958**, *110*, 1.
(58) Schaefer, D. W. *J. Chem. Phys.* **1977**,*66*, 3980.
(59) Hayter, J. B.; Penfold, J. *Mol. Phys.* **1981**, *42*, 109.
(60) Dubin, S. B.; Clark, N. A.; Benedek, G. B. *J. Chem. Phys.* **1971**, *54*, 5158.
(61) Thiele, E. *J. Chem. Phys.* **1968**, *39*, 474.
(62) Wertheim, M. S. *Phys. Rev. Lett.* **1963**, *10*, 321.
(63) Muschol, M.; Rosenberger, F. *J. Chem. Phys.* **1995**, *103*, 10424.
(64) Chipman, D. M.; Sharon, N. *Science* **1969**, *165*, 454.
(65) Krigbaum, W. R.; Kügler F. R. *Biochemistry* **1970**, *9*, 1216.
(66) Svergun, D. I.; Richard, C.; Koch, M. H. J.; Sayers, Z.; Kuprin, S.; Zaccai, G. *Proc. Natl. Acad. Sci. U.S.A.* **1998**, *95*, 2367.
(67) Ducruix, A.; Guilloteau, J. P.; Riès-Kautt, M.; Tardieu, A. *J. Cryst. Growth* **1996**, *168*, 28.
(68) Tanford, C. *Physical Chemistry of Macromolecules*; Wiley: New York, 1961.
(69) Price, W. S.; Tsuchiya, F.; Arata, Y *J. Am. Chem. Soc.* **1999**, *121*, 11503.
(70) Eberstein, W.; Georgalis, Y.; Saenger, W. *J. Cryst. Growth* **1994**, *143*, 71.
(71) Durchschlag, H.; Zipper, P. *J. Com. Esp. Deterg.* **1995**, *26*, 275.
(72) *Intermolecular and Surface Forces*; Israelachvili, J., Ed.; Academic Press: New York 1992.